Journal of Statistical Mechanics:
Theory and Experiment

PAPER

One-component fermion plasma on a sphere at finite temperature: the anisotropy of the path conformations

Journal of Statistical Mechanics: Theory and Experiment
An IOP and SISSA journal

PAPER: Quantum statistical physics, condensed matter, integrable systems

One-component fermion plasma on a sphere at finite temperature: the anisotropy of the path conformations

Riccardo Fantoni*

Dipartimento di Fisica, Università di Trieste, strada Costiera 11, 34151 Grignano Trieste, Italy
E-mail: riccardo.fantoni@posta.istruzione.it

Received 27 March 2023
Accepted for publication 18 July 2023
Published 16 August 2023

Online at stacks.iop.org/JSTAT/2023/083103
https://doi.org/10.1088/1742-5468/aceb54

Abstract. In our previous work (Fantoni 2018 *Int. J. Mod. Phys.* C **29** 1850064) we studied, through a computer experiment, a one-component fermion plasma on a sphere at finite, non-zero temperature. We extracted thermodynamic properties, such as the kinetic and internal energy per particle, and structural properties, such as the radial distribution function, and produced some snapshots of the paths to study their shapes. Here, we revisit this study, giving more theoretical details explaining the path shape anisotropic conformation due to the inhomogeneity in the polar angle of the variance of the random walk diffusion from the kinetic action.

Keywords: one-component plasma, Monte Carlo simulation, finite temperature, restricted path integral, fermion sign problem, observables, path shape conformation

*Author to whom any correspondence should be addressed.

 1742-5468/23/083103+12$33.00

Contents

1. Introduction

In our work in [1] we studied, through restricted path integral Monte Carlo, a one-component fermion plasma on a sphere of radius a at finite, non-zero, absolute temperature T. We extracted thermodynamic properties like the kinetic and internal energy per particle and structural properties like the radial distribution function, and produced some snapshots of the paths to study their shapes.

Our results extend to the quantum regime the previous non-quantum results obtained for the analytically exactly solvable plasma on curved surfaces [2–7] and for its numerical Monte Carlo experiment [8]. In particular, we show how the configuration space (see figure 1 of [1]) appears much more complicated than in the classical case (see figures 5 and 6 of [8]). The first notable phenomenon is the fact that whereas the particle distribution is certainly isotropic, the path conformation is not. Some paths tend to wind around the sphere running along the parallels in proximity to the poles, while others run along the meridians in proximity to the equator. This is a direct consequence of the coordinate dependence of the variance of the diffusion. At high temperatures, the paths tend to be localized, whereas at low temperatures, they tend to be delocalized and distributed over a larger part of the surface with long links between the beads.

The plasma is an ensemble of point-wise electrons that interact through the Coulomb potential, assuming that the electric field lines can permeate the three-dimensional space where the sphere is embedded. The system of particles is thermodynamically stable even if the pair-potential is purely repulsive because the particles are confined to the compact surface of the sphere, and we do not need to add a uniform neutralizing background as in the Wigner Jellium model [9–13]. Therefore, our spherical plasma made of N spinless indistinguishable electrons of charge $-e$ and mass m will carry a total negative charge $-Ne$, a total mass Nm, and will have a radius a.

In this work, we conduct a thought computer experiment such as the one carried out in [1] in order to extract some theoretical conclusions on the path shape and conformation and try to explain the results found in [1].

Our study can be used to predict the properties of a metallic spherical shell, such as a spherical shell of graphene. Today, we assisted to a rapid development of the laboratory

J. Stat. Mech. (2023) 083103

realization of graphene hollow spheres [14, 15] with many technological interests. These are used as electrodes for supercapacitors and batteries, as superparamagnetic materials, as electrocatalysts for oxygen reduction, in drug delivery, and as a conductive catalyst for photovoltaic applications [16–24]. Of course, with simulation we can access the more various and extreme conditions otherwise not accessible in a laboratory.

A possible further study would be the simulation of the neutral sphere, where we model the plasma of electrons embedded in a spherical shell that is uniformly positively charged in such a way that the system is globally neutrally charged. This could easily be done by changing the Coulomb pair-potential into $e^2/r \to e^2(1/r-1)$. In the $a\to\infty$ limit, this would reduce to the Wigner Jellium model that has received much attention lately, from the point of view of a path integral Monte Carlo simulation [1, 25–33]. Alternatively, we could study the two-component plasma on the sphere, as has recently been done in the tridimensional Euclidean space [33]. Another possible extension of our work is the realization of the simulation of the full anyonic plasma on the sphere, taking appropriate care of the fractional statistics and the phase factors to append to each disconnected region of the path integral expression for the partition function [1]. This could become important in a study of the quantum Hall effect by placing a magnetic Dirac monopole at the center of the sphere [34, 35]. In addition, the adaptation of our simulation to a fully relativistic Hamiltonian could be of some interest in the study of graphinos.

The paper is organized as follows: in section 2 we describe the thought system and the method used for its study, in section 3 we present our theoretical study and predictions, and section 4 contains the concluding discussion.

2. The problem

A point $\mathbf{q}$ on the sphere of radius a, the surface of constant positive curvature, is given by

$$\boldsymbol{r}/a = \sin\theta\cos\varphi\hat{\boldsymbol{x}} + \sin\theta\sin\varphi\hat{\boldsymbol{y}} + \cos\theta\hat{\boldsymbol{z}}, \tag{2.1}$$

where θ is the polar angle and φ is the azimuthal angle. The N particle positions are at $\boldsymbol{R} = (\boldsymbol{r}_1, \boldsymbol{r}_2, \ldots, \boldsymbol{r}_N)$. The surface density of the plasma will then be $\sigma = N/4\pi a^2$. On the sphere we have the following metric:

$$\mathrm{d}s^2 = g_{\mu\nu}\mathrm{d}q^\mu\mathrm{d}q^\nu = a^2\left[\mathrm{d}\theta^2 + \sin^2\theta\mathrm{d}\varphi^2\right], \tag{2.2}$$

where Einstein summation convention on repeated indices is assumed. We will use Greek indices for either the surface components or the surface components of each particle coordinate and Roman indices for either the particle index or the time-slice index, $q^1 = \theta \in [0,\pi)$, $q^2 = \varphi \in [-\pi,\pi)$, and the positive definite and symmetric metric tensor is given by

$$g_{\mu\nu} = \begin{pmatrix} a^2 & 0 \\ 0 & a^2\sin^2\theta \end{pmatrix}. \tag{2.3}$$

J. Stat. Mech. (2023) 083103

We have periodic boundary conditions in $\theta+\pi=\theta$ and in $\varphi+2\pi=\varphi$. We will also define $\boldsymbol{Q}=(\boldsymbol{q}_1,\boldsymbol{q}_2,\ldots,\boldsymbol{q}_N)$. The geodesic distance between two infinitesimally close points $\mathbf{Q}$ and $\boldsymbol{Q}'$ is $\mathrm{d}s^2(\boldsymbol{Q},\boldsymbol{Q}')=\sum_{i=1}^N \mathrm{d}s^2(\boldsymbol{q}_i,\boldsymbol{q}_i')$, where the geodesic distance between the points $\mathbf{q}$ and $\boldsymbol{q}'$ on the sphere is

$$s(\boldsymbol{q},\boldsymbol{q}')=a\arccos\left[\cos(q^1)\cos({q^1}')+\sin(q^1)\sin({q^1}')\cos(q^2-{q^2}')\right]. \tag{2.4}$$

The Hamiltonian of the N non-relativistic indistinguishable particles of the one-component spinless fermion plasma is given by

$$\mathcal{H}=\mathcal{T}+\mathcal{V}=-\lambda\sum_{i=1}^N\Delta_i+\sum_{i<j}v_{ij}, \tag{2.5}$$

with $\lambda=\hbar^2/2m$, where m is the electron mass, and $\Delta_i=g_i^{-1/2}\partial(g_i^{1/2}g_i^{\mu\nu}\partial/\partial q_i^\nu)/\partial q_i^\mu$ the Laplace–Beltrami operator for the ith particle on the sphere of radius a in local coordinates, where $g_{\mu\alpha}g^{\alpha\nu}=\delta_\mu^\nu$ and $g_i=\det||g_{\mu\nu}(\boldsymbol{q}_i)||$. We have assumed that $\mathcal{H}$ in curved space has the same form as in flat space. For the pair-potential, v, we will choose

$$v_{ij}=e^2/r_{ij}, \tag{2.6}$$

where e is the electron charge and r_{ij} is the Euclidean distance between two particles at $\mathbf{q}_i$ and $\mathbf{q}_j$, which is given by

$$r_{ij}=a\sqrt{2-2\hat{\boldsymbol{r}}_i\cdot\hat{\boldsymbol{r}}_j}=2a\sin[\arccos(\hat{\boldsymbol{r}}_i\cdot\hat{\boldsymbol{r}}_j)/2], \tag{2.7}$$

where $\hat{\boldsymbol{r}}_i=\boldsymbol{r}_i/a$ is the versor that from the center of the sphere points toward the center of the ith particle. So, the electrons *move on* a spherical shell with the electric field lines permeating the surrounding three-dimensional space, but they do not *live in* the shell.

Given the antisymmetrization operator $\mathcal{A}=\sum_P/N!$, where the sum runs over all particle permutations P, and the inverse temperature $\beta=1/k_\mathrm{B}T$, where k_B is Boltzmann's constant, the one-component fermion plasma density matrix, $\rho_\mathrm{F}=\mathcal{A}\mathrm{e}^{-\beta\mathcal{H}}$, in the coordinate representation, on a generic Riemannian manifold of metric g [5, 36], is

$$\rho_\mathrm{F}(\boldsymbol{Q}',\boldsymbol{Q};\beta)=\int\rho_\mathrm{F}(\boldsymbol{Q}',\boldsymbol{Q}((M-1)\tau);\tau)\cdots\rho_\mathrm{F}(\boldsymbol{Q}(\tau),\boldsymbol{Q};\tau)\prod_{j=1}^{M-1}\sqrt{\tilde{g}_{(j)}}\prod_{i=1}^N\mathrm{d}q_i^1(j\tau)\wedge\mathrm{d}q_i^2(j\tau)\ , \tag{2.8}$$

where as usual we discretize the *imaginary thermal time* in bits $\tau=\hbar\beta/M$. We will often use the following shorthand notation for the *path integral* measure: $\prod_{j=1}^{M-1}\sqrt{\tilde{g}_{(j)}}\prod_{i=1}^N \mathrm{d}q_i^1(j\tau)\wedge\mathrm{d}q_i^2(j\tau)\to\mathcal{D}\boldsymbol{Q}$ as $M\to\infty$. The path of the ith particle is given by $\{\boldsymbol{q}_i(t)|t\in[0,\hbar\beta]\}$ with t the imaginary thermal time. Each $\boldsymbol{q}_i(j\tau)$ with $i=1,\ldots,N$ and $j=1,\ldots,M$ represents the various *beads* forming the discretized path. The N particle path

J. Stat. Mech. (2023) 083103

is given by $\{\boldsymbol{Q}(t)|t\in[0,\hbar\beta]\}$. Moreover,

$$\tilde{g}_{(j)}=\det||\tilde{g}_{\mu\nu}(\boldsymbol{Q}(j\tau))||,\quad j=1,2,\ldots,M-1, \tag{2.9}$$

$$\tilde{g}_{\mu\nu}(\boldsymbol{Q})=g_{\alpha_1\beta_1}(\boldsymbol{q}_1)\otimes\ldots\otimes g_{\alpha_N\beta_N}(\boldsymbol{q}_N), \tag{2.10}$$

In the small τ limit, we have

$$\rho_{\mathrm{F}}(\boldsymbol{Q}(2\tau),\boldsymbol{Q}(\tau);\tau)\propto\mathcal{A}\left[\tilde{g}_{(2)}^{-1/4}\sqrt{D(\boldsymbol{Q}(2\tau),\boldsymbol{Q}(\tau);\tau)}\tilde{g}_{(1)}^{-1/4}\mathrm{e}^{\lambda\tau R(\boldsymbol{Q}(\tau))/6\hbar}\mathrm{e}^{-\frac{1}{\hbar}S(\boldsymbol{Q}(2\tau),\boldsymbol{Q}(\tau);\tau)}\right], \tag{2.11}$$

where $\mathcal{A}$ can act on the first, the second, or on both *time slices*. $R(\boldsymbol{Q})$ is the scalar curvature of the curved manifold, S is the action and D is van Vleck's determinant

$$D_{\mu\nu}=\frac{\partial^2S(\boldsymbol{Q}(2\tau),\boldsymbol{Q}(\tau);\tau)}{\partial Q^\mu(2\tau)\partial Q^\nu(\tau)}, \tag{2.12}$$

$$\det||D_{\mu\nu}||=D(\boldsymbol{Q}(2\tau),\boldsymbol{Q}(\tau);\tau), \tag{2.13}$$

where here the Greek index denotes the two components of each particle coordinate.

For the *action* and the *kinetic action*, we have

$$S(\boldsymbol{Q}',\boldsymbol{Q})=K(\boldsymbol{Q}',\boldsymbol{Q})+U(\boldsymbol{Q}',\boldsymbol{Q}), \tag{2.14}$$

$$K(\boldsymbol{Q}',\boldsymbol{Q})=N\hbar\ln(4\pi\lambda\tau/\hbar)+\frac{\hbar^2s^2(\boldsymbol{Q}',\boldsymbol{Q})}{4\lambda\tau}, \tag{2.15}$$

where in the *primitive approximation* [37] we find the following expression for the *interaction*,

$$U(\boldsymbol{Q}',\boldsymbol{Q})=\frac{\tau}{2}[V(\boldsymbol{Q}')+V(\boldsymbol{Q})], \tag{2.16}$$

$$V(\boldsymbol{Q})=\sum_{i<j}v_{ij}. \tag{2.17}$$

In particular, the kinetic action is responsible for the diffusion of the random walk with a variance of $2\lambda\tau g^{\mu\nu}/\hbar$.

On the sphere, we have $R=N\mathcal{R}$ with $\mathcal{R}=2/a^2$, the scalar curvature of the sphere of radius a, and in the $M\to\infty$ limit $s^2(\boldsymbol{Q}',\boldsymbol{Q})\to\mathrm{d}s^2(\boldsymbol{Q}',\boldsymbol{Q})$ and $\tilde{g}_{(2)}^{-1/4}\sqrt{D(\boldsymbol{Q}(2\tau),\boldsymbol{Q}(\tau);\tau)}\,\tilde{g}_{(1)}^{-1/4}\to\left(\hbar^2/2\lambda\tau\right)^N$ [38]. We recover the Feynman–Kac path integral formula on the sphere in the $\tau\to0$ limit. We will then have to deal with $2NM$ multidimensional integrals for which Monte Carlo [39] is a suitable computational method. For example, to measure an observable $\mathcal{O}$ we need to calculate the following quantity:

$$\langle\mathcal{O}\rangle=\frac{\int O(\boldsymbol{Q},\boldsymbol{Q}')\rho_F(\boldsymbol{Q}',\boldsymbol{Q};\beta)\,\mathrm{d}\boldsymbol{Q}\mathrm{d}\boldsymbol{Q}'}{\int\rho_{\mathrm{F}}(\boldsymbol{Q},\boldsymbol{Q};\beta)\,\mathrm{d}\boldsymbol{Q}}, \tag{2.18}$$

J. Stat. Mech. (2023) 083103

where $\sqrt{\tilde{g}}\prod_{i=1}^{N} \mathrm{d}q_i^1 \wedge \mathrm{d}q_i^2 \equiv \mathrm{d}\boldsymbol{Q}$. Notice that most of the properties that we will measure are diagonal in coordinate representation, requiring then just the diagonal density matrix, $\rho_{\mathrm{F}}(\boldsymbol{Q},\boldsymbol{Q};\beta)$.

For example, for the density $\rho(\boldsymbol{q}) = \langle \mathcal{O} \rangle$ with

$$O(\boldsymbol{Q};\boldsymbol{q}) = \sum_{i=1}^{N} \delta^{(2)}(\boldsymbol{q}-\boldsymbol{q}_i), \tag{2.19}$$

where $\delta^{(2)}(\boldsymbol{q}) = \delta(q^1)\delta(q^2)$ and δ is the Dirac delta function. Clearly $\int \sigma(\boldsymbol{q})\sqrt{g(\boldsymbol{q})}\mathrm{d}\boldsymbol{q} = N$ and a uniform distribution of electrons is signaled by a constant density throughout the surface of the sphere.

Fermion properties cannot be calculated exactly with the path integral Monte Carlo because of the fermion sign problem [40, 41]. We then have to resort to an approximated calculation. The one we chose in [1] was the restricted path integral approximation [40, 41] with a 'free fermion restriction'. The trial density matrix used in the restriction is chosen as the one reducing to the ideal density matrix in the limit of $t \ll 1$, and is given by

$$\rho_0(\boldsymbol{Q}',\boldsymbol{Q};t) \propto \mathcal{A}\left\| \mathrm{e}^{-\frac{\hbar s^2(\boldsymbol{q}_i',\boldsymbol{q}_j)}{4\lambda t}} \right\|. \tag{2.20}$$

The *restricted path integral identity* that can be used [40, 41] is as follows: mathindent0pt

$$\rho_{\mathrm{F}}(\boldsymbol{Q}',\boldsymbol{Q};\beta) \propto \int \sqrt{\tilde{g}''}\mathrm{d}\boldsymbol{Q}''\,\rho_{\mathrm{F}}(\boldsymbol{Q}'',\boldsymbol{Q};0) \oint_{\boldsymbol{Q}''\to\boldsymbol{Q}'\in\gamma_0(\boldsymbol{Q})} \mathcal{D}\boldsymbol{Q}'''\,\mathrm{e}^{-S[\boldsymbol{Q}''']/\hbar}, \tag{2.21}$$

where S is the Feynman–Kac action

$$S[\boldsymbol{Q}] = \int_0^{\hbar\beta} \mathrm{d}t \left[\frac{\hbar^2}{4\lambda} \dot{\boldsymbol{Q}}_\mu \dot{\boldsymbol{Q}}^\mu + V(\boldsymbol{Q}) \right], \tag{2.22}$$

where the dot indicates a total derivative with respect to the imaginary thermal time, and the subscript in the path integral of equation (2.21) means that we restrict the path integration to paths starting at $\boldsymbol{Q}''$, ending at $\boldsymbol{Q}'$ and avoiding the nodes of ρ_0, that is to the *reach* of $\mathbf{Q}$, γ_0. The nodes are on the reach boundary $\partial\gamma_0$. The weight of the walk is $\rho_{\mathrm{F}}(\boldsymbol{Q}'',\boldsymbol{Q};0) = \mathcal{A}\delta(\boldsymbol{Q}''-\boldsymbol{Q}) = (N!)^{-1}\sum_{\mathcal{P}}(-)^{\mathcal{P}}\ \delta^{(2N)}(\boldsymbol{Q}''-\mathcal{P}\boldsymbol{Q})$, where the sum is over all the permutations $\mathcal{P}$ of the N fermions, $(-)^{\mathcal{P}}$ is the permutation sign, positive for an even permutation and negative for an odd permutation, and δ is a Dirac delta function. It is clear that the contribution of all the paths for a single element of the density matrix will be of the same sign, thus solving the sign problem; it is positive if $\rho_{\mathrm{F}}(\boldsymbol{Q}'',\boldsymbol{Q};0) > 0$, and negative otherwise. On the diagonal, the density matrix is positive and on the path restriction $\rho_{\mathrm{F}}(\boldsymbol{Q}',\boldsymbol{Q};\beta) > 0$ then only even permutations are allowed since $\rho_{\mathrm{F}}(\boldsymbol{Q},\mathcal{P}\boldsymbol{Q};\beta) = (-)^{\mathcal{P}}\rho_{\mathrm{F}}(\boldsymbol{Q},\boldsymbol{Q};\beta)$. It is then possible to use a boson calculation to get the fermion case. Clearly, the restricted path integral identity with the free fermion restriction becomes exact if we simulate free fermions, but otherwise is just an approximation. The approximation is expected to improve at low density and high temperature, i.e. when correlation effects are weak. The implementation of the restricted, fixed-node, path integral identity within the worm algorithm was also the subject of our previous study on the three-dimensional Euclidean Jellium [11].

In [1] we worked in the grand canonical ensemble with fixed chemical potential μ, surface area $A = 4\pi a^2$, and absolute temperature T. At a higher value of the chemical potential we will have a higher number of particles on the surface and a higher density. On the other hand, increasing the radius of the sphere at constant chemical potential will produce a plasma with lower surface density. The *Coulomb coupling constant* is $\Gamma = \beta e^2/a_0 r_s$ with $a_0 = \hbar^2/me^2$ the Bohr radius and $r_s = (4\pi\sigma)^{-1/2}/a_0$. At weak coupling, $\Gamma \ll 1$, the plasma becomes weakly correlated and approaches the ideal gas limit. This will occur at high temperatures and/or low densities. The *electron degeneracy parameter* is $\Theta = T/T_\mathrm{D}$, where the degeneracy temperature $T_\mathrm{D} = \sigma\hbar^2/mk_\mathrm{B}$. For temperatures higher than T_D, $\Theta \gg 1$, the quantum effects are less relevant.

3. Theoretical study

In order to understand the anisotropic conformation of the path snapshots and their dependence on the azimuthal angle φ and polar angle θ, we observe that in the primitive approximation we have in the path integral a weight factor $\propto \exp(-\hbar \mathrm{d}s^2/4\lambda\tau)$ stemming from the kinetic part of the action, where $\mathrm{d}s^2$ is given by equation (2.2). In particular, we see that if we are near the poles, $\theta \approx 0$ or π, then $\mathrm{d}s^2 \approx a^2\mathrm{d}\theta^2$ and we see that it costs nothing to change the azimuthal angle. This explains the paths winding along the parallels in proximity to the poles. On the other hand, near the equator, at $\theta \approx \pi/2$, we find $\mathrm{d}s^2 \approx a^2(\mathrm{d}\theta^2 + \mathrm{d}\varphi^2)$ so that the paths will tend to wander around the equator in no particular direction.

The same can be seen when studying the behavior of the finite geodesic distance of equation (2.5). In figure 1 we show a three-dimensional plot for $\theta' = 0.2$ and $\varphi' = 0$. Again, we see that around the pole at $\theta \approx 0$ it costs nothing to change φ, that is, to go along a parallel, while a path traveling along a meridian will be unfavored since we need to increase θ. In figure 2 we show a three-dimensional plot for $\theta' = \pi/2$ and $\varphi' = 0$. We now see that around the equator at $\theta \approx \pi/2$ a path wandering around the initial position is favored, with no preferred direction along the parallels or the meridians.

Clearly, if we rotate the sphere, the path shape will simply rotate following the rotation of its poles. This anisotropy of the path conformations is rather counter-intuitive since the sphere is notoriously isotropic, but it reflects the inhomogeneity of the metric with respect to the polar angle.

It is important to distinguish the effect that we just described due to the weight factor $\propto \exp(-\hbar \mathrm{d}s^2/4\lambda\tau)$ stemming from the kinetic part of the primitive action from the measure factor $\prod_{j=1}^{M}\sqrt{\tilde{g}(j)}$ also entering the path integral. This last factor, being also independent of the azimuthal angles, will produce the same local density $\rho(\boldsymbol{q})$ under a rotation of the sphere around its axis through the poles. As a result, by isotropy, we conclude that the density must be a constant under any rotation, which means that the plasma must be uniform [5].

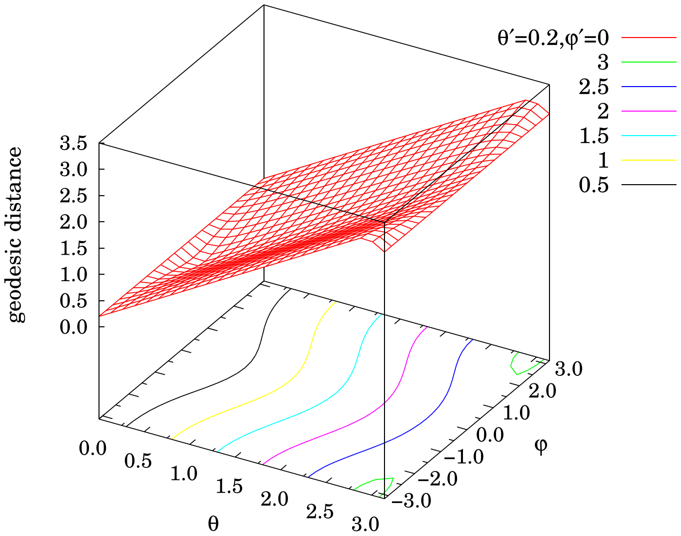

Figure 1. Three-dimensional plot of the geodesic distance of equation (2.5) for $\theta' = 0.2$ and $\varphi' = 0$. From the surface graph we see how in the proximity of the poles the geodesic distance between points moving along parallels is small, while it increases rapidly if one moves along the meridians.

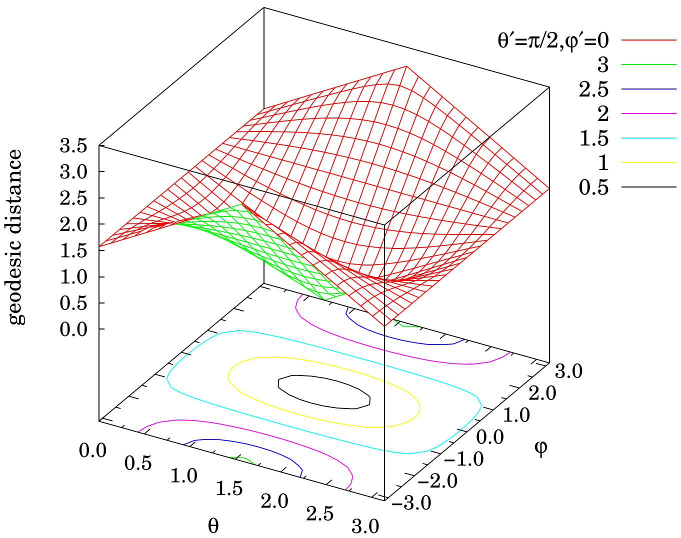

Figure 2. Three-dimensional plot of the geodesic distance of equation (2.5) for $\theta' = \pi/2$ and $\varphi' = 0$. From the surface graph we see how in the proximity of the equator the geodesic distance between points moving in circles in the (θ, φ) plane is small, while it increases rapidly if one moves along the parallels.

The temperature dependence can also be easily explained. At high temperature, β is small, $\Theta \gg 1$, and the path extending from $t = 0$ to $t = \hbar\beta$ will be localized, of a small size, and quantum effects will be less relevant. Meanwhile, at low temperature, β is large, $\Theta \ll 1$, and the path will be delocalized, increased in size, it diffuses more

J. Stat. Mech. (2023) 083103

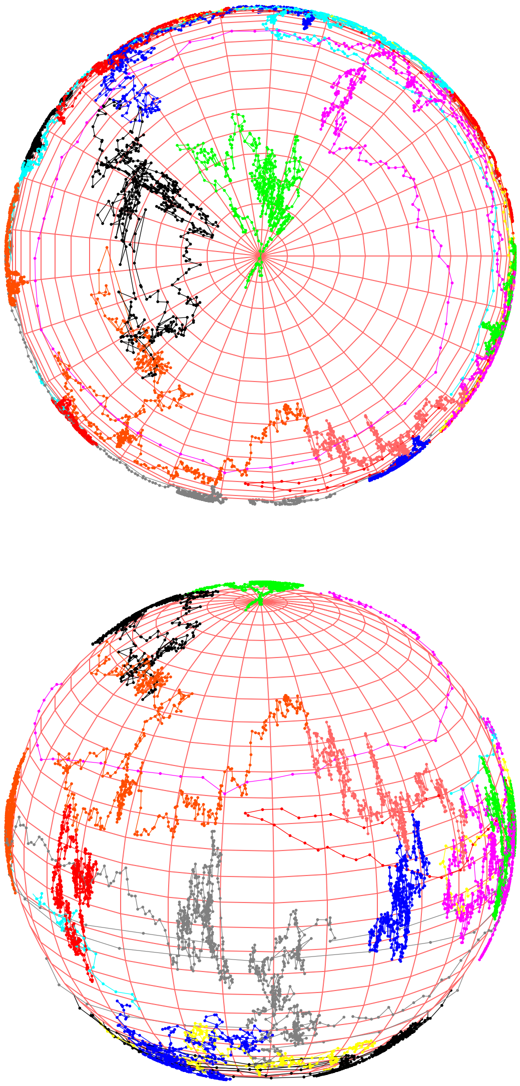

Figure 3. Snapshot of the macroscopic path during a simulation. The different paths have different colors. The simulation parameters specifying the thermodynamic conditions are as follows: $a = 5, \lambda = 1, \beta = 5, \mu = 8$.

on the surface, and quantum effects are more relevant. Usually, we are interested in measuring observables that are diagonal so that when dealing with the diagonal density matrix $\rho_{\mathrm{F}}(\boldsymbol{Q}, \boldsymbol{Q}; \beta)$ we will observe *ring* paths, such that $\boldsymbol{Q}(0) = \boldsymbol{Q}(\hbar\beta)$. Moreover, at high temperature, the diagonal density matrix will involve almost straight localized ring paths closing themselves on the identity permutation. At low temperatures, the delocalized paths will eventually wind through the $\hbar\beta$ periodicity by means of several different permutations $\mathcal{P}$, so that $\boldsymbol{Q}(0) = \mathcal{P}\boldsymbol{Q}(\hbar\beta)$ and so on. Any permutation can be broken into a product of cyclic permutations. Each cycle corresponds to several paths 'cross-linking' and forming a larger ring path. Quantum mechanically, the plasma does

J. Stat. Mech. (2023) 083103

this to lower its kinetic energy. According to Feynman's 1953 theory [37], the superconductor transition is represented by the formation of macroscopic paths, i.e. those stretching across the whole sphere and involving on the order of N electrons. In other words, the ring paths percolate through the periodic boundary conditions $\theta = \theta + \pi$ and $\varphi = \varphi + 2\pi$ by means of permutations.

In figure 3 we show a snapshot of the macroscopic path during a simulation of [1].

4. Conclusions

In this work we revised our restricted path integral Monte Carlo simulation [1] of a one-component spinless fermion plasma at finite, non-zero temperature on the surface of a sphere. The Coulomb interaction is e^2/r with r the Euclidean distance between two electrons of elementary charge e (we could also have chosen instead of r the geodesic distance, s, within the sphere). This gives us an approximated numerical solution of the many-body problem. The exact solution cannot be accessed due to the fermion sign catastrophe. Impenetrable indistinguishable particles on the surface of a sphere admit, in general, anyonic statistics [42]. Here, we just project the larger braid group onto the permutation group and choose the fermion sector for our study.

The path integral Monte Carlo method chosen in [1] used the primitive approximation for the action, which can be improved, for example, by the use of the pair-product action [37]. The restriction was carried out choosing as guiding trial density matrix the one of ideal free fermions. This choice would of course return an exact solution for the simulation of ideal fermions, but it furnishes just an approximation for the interacting coulombic plasma.

In this work we showed how the conformation anisotropy of the paths observed in the simulations of [1] can be explained through the inhomogeneous nature of the metric in the polar angle, or equivalently, from the inhomogeneous nature of the geodesic distance on the surface of the sphere. This is ultimately due to the fact that the metric enters with the negative sign in the exponent of the primitive approximation of the density matrix. We should not confuse the anisotropy in the path conformation with the fact that the plasma will always be homogeneous (with a constant local density ρ) on the sphere. In the degenerate regime (low T) the observed strong anisotropy in the path conformation near the poles or the equator of the sphere should also be due to a peculiar behavior in the properties of the N-particle off-diagonal density matrix. This, as is well known, is directly related to a number of physical properties, such as the quasi-particle excitation spectrum and the momentum distribution. Therefore, the system properties can deviate significantly from just a pure homogeneous 2D system, and the inhomogeneous nature of the space metric is of particular importance.

We also suggest the possibility to observe a superconducting plasma at low temperature when we observe ring paths percolating through the periodic boundary conditions $\theta = \theta + \pi$ and $\varphi = \varphi + 2\pi$ by means of permutations, even if some care has to be addressed to take into account the peculiar asymptotic behavior of the one-particle density matrix.

J. Stat. Mech. (2023) 083103

References

[1] Fantoni R 2018 One-component fermion plasma on a sphere at finite temperature *Int. J. Mod. Phys.* C **29** 1850064
[2] Fantoni R, Jancovici B and Téllez G 2003 Pressures for a one-component plasma on a pseudosphere *J. Stat. Phys.* **112** 27
[3] Fantoni R and Téllez G 2008 Two dimensional one-component plasma on a Flamm's paraboloid *J. Stat. Phys.* **133** 449
[4] Fantoni R 2012 Two component plasma in a Flamm's paraboloid *J. Stat. Mech.* **2012** 04015
[5] Fantoni R 2012 The density of a fluid on a curved surface *J. Stat. Mech.* **2012** 10024
[6] Fantoni R 2016 Exact results for one dimensional fluids through functional integration *J. Stat. Phys.* **163** 1247
[7] Fantoni R 2017 The moment sum-rules for ionic liquids at criticality *Physica* A **477C** 187
[8] Fantoni R, Salari J W O and Klumperman B 2012 The structure of colloidosomes with tunable particle density: simulation vs experiment *Phys. Rev.* E **85** 061404
[9] Fantoni R and Tosi M P 1995 Coordinate space form of interacting reference response function of d-dimensional jellium *Il Nuovo Cimento* D **17D** 1165
[10] Fantoni R 2013 Radial distribution function in a diffusion monte carlo simulation of a fermion fluid between the ideal gas and the jellium model *Eur. Phys. J.* B **86** 286
[11] Fantoni R 2021 Jellium at finite temperature using the restricted worm algorithm *Eur. Phys. J.* B **94** 63
[12] Fantoni R 2021 Form invariance of the moment sum-rules for jellium with the addition of short-range terms in the pair-potential *Indian J. Phys.* **95** 1027
[13] Fantoni R 2021 Jellium at finite temperature *Mol. Phys.* **120** 4
[14] Rashid A and Yusoff M (eds) 2015 *Graphene-Based Energy Devices* (Wiley)
[15] Tiwari A and Syväjärvi M (eds) 2015 *Graphene Materials: Fundamentals and Emerging Applications* (Scrivener Publishing)
[16] Guo P, Song H and Chena X 2010 Hollow graphene oxide spheres self-assembled by W/O emulsion *J. Mater. Chem.* **20** 4867
[17] Cao J, Wang Y, Xiao P, Chen Y, Zhou Y, Ouyang J-H and Jia D 2013 Hollow graphene spheres self-assembled from graphene oxide sheets by a one-step hydrothermal process *Carbon* **56** 389
[18] Wu L, Feng H, Liu M, Zhang K and Li J 2013 Graphene-based hollow spheres as efficient electrocatalysts for oxygen reduction *Nanoscale* **5** 10839
[19] Shao Q, Tang J, Lin Y, Zhang F, Yuan J, Zhang H, Shinyaa N and Qinc L-C 2013 Synthesis and characterization of graphene hollow spheres for application in supercapacitors *J. Mater. Chem.* A **1** 15423
[20] Zhao Y, Chen M and Wu L 2016 Recent progress in hollow sphere-based electrodes for high-performance supercapacitors *Nanotechnology* **27** 342001
[21] Cho J S, Lee J-K and Y C Yong 2016 Graphitic carbon-coated $FeSe_2$ hollow nanosphere-decorated reduced graphene oxide hybrid nanofibers as an efficient anode material for sodium ion batteries *Sci. Rep.* **6** 23699
[22] Hao D, Xuefen C, Liangdong Q and Xiaohui Z 2016 Fabrication, characterization and properties of superparamagnetic reduced graphene oxide/Fe_3O_4 hollow sphere nanocomposites *Rare Met. Mater. Eng.* **45** 1669
[23] Huang W, Ding S, Chen Y, Hao W, Lai X, Peng J, Tu J, Cao Y and Li X 2017 3D NiO hollow sphere/reduced graphene oxide composite for high-performance glucose biosensor *Sci. Rep.* **7** 5220
[24] Bi E, Chen H, Yang X, Ye F, Yin M and Han L 2017 Fullerene-structured $MoSe_2$ hollow spheres anchored on highly nitrogen-doped graphene as a conductive catalyst for photovoltaic applications *Sci. Rep.* **5** 5220
[25] Brown E W, Clark B K, DuBois J L and Ceperley D M 2013 Path-integral Monte Carlo simulation of the warm dense homogeneous electron gas *Phys. Rev. Lett.* **110** 146405
[26] Brown E, Morales M A, Pierleoni C and Ceperley D M *et al* 2014 Quantum Monte Carlo techniques and applications for warm dense matter *Frontiers and Challenges in Warm Dense Matter* ed F Graziani (Springer) pp 123–49
[27] Dornheim T, Groth S, Sjostrom T, Malone F D, Foulkes W M C and Bonitz M 2016 *Ab initio* quantum Monte Carlo simulation of the warm dense electron gas in the thermodynamic limit *Phys. Rev. Lett.* **117** 156403
[28] Dornheim T, Groth S, Schoof T, Hann C and Bonitz M 2016 *Ab initio* quantum Monte Carlo simulations of the uniform electron gas without fixed nodes: the unpolarized case *Phys. Rev.* B **93** 205134
[29] Groth S, Schoof T, Dornheim T and Bonitz M 2016 *Ab initio* quantum Monte Carlo simulations of the uniform electron gas without fixed nodes *Phys. Rev.* B **93** 085102

J. Stat. Mech. (2023) 083103

[30] Groth S, Dornheim T, Sjostrom T, Malone F D, Foulkes W M C and Bonitz M 2017 *Ab initio* exchange-correlation free energy of the uniform electron gas at warm dense matter conditions *Phys. Rev. Lett.* **119** 135001
[31] Malone F D, Blunt N S, Brown E W, Lee D K K, Spencer J S, Foulkes W M C and Shepherd J J 2016 Accurate exchange-correlation energies for the warm dense electron gas *Phys. Rev. Lett.* **117** 115701
[32] Filinov V S, Fortov V E, Bonitz M and Moldabekov Z 2015 Fermionic path-integral Monte Carlo results for the uniform electron gas at finite temperature *Phys. Rev.* E **91** 033108
[33] Fantoni R 2018 Two component boson–fermion plasma at finite temperature *Int. J. Mod. Phys.* C **29** 1850028
[34] Melik-Alaverdian V, Bonesteel N E and Ortiz G 1997 Fixed-phase diffusion Monte Carlo study of the quantum-hall effect on the haldane sphere *Phys. Rev. Lett.* **79** 5286
[35] Melik-Alaverdian V, Ortiz G and Bonesteel N E 2001 Quantum projector method on curved manifolds *J. Stat. Phys.* **104** 449
[36] Schulman L S 1981 *Techniques and Applications of Path Integrals* (Wiley) ch 24
[37] Ceperley D M 1995 Path integrals in the theory of condensed helium *Rev. Mod. Phys.* **67** 279
[38] For a space of constant curvature there is clearly no effect, as the term due to the curvature just leads to a constant multiplicative factor that has no influence on the measure of the various observables. One might have hoped that certain constrained coordinates, perhaps a relative coordinate in a molecule, would effectively live in a space of variable curvature. Perhaps gravitation will give us the system on which the effect of curvature can be seen, but at present the effect is purely in the realm of theory
[39] Kalos M H and Whitlock P A 2008 *Monte Carlo Methods* (Wiley)
[40] Ceperley D M 1991 Fermion nodes *J. Stat. Phys.* **63** 1237
[41] Ceperley D M 1996 Path integral Monte Carlo methods for fermions *Monte Carlo and Molecular Dynamics of Condensed Matter Systems* ed K Binder and G Ciccotti (Editrice Compositori)
[42] Fantoni R 2021 How should we choose the boundary conditions in a simulation which could detect anyons in one and two dimensions? *J. Low Temp. Phys.* **202** 247

J. Stat. Mech. (2023) 083103